Genetic architecture of a mutation's expressivity and penetrance

Rachel Schell[1], Martin N. Mullis[1], Takeshi Matsui[1,2], Ryan Foree[1], and Ian M. Ehrenreich[1,*]

[1] Molecular and Computational Biology Section, Department of Biological Sciences, University of Southern California, Los Angeles, CA 90089, USA

[2] Present address: Joint Initiative for Metrology in Biology, Stanford, CA 94305, USA

* Correspondence to:
Ian M. Ehrenreich
Phone #: 213 – 821 – 5349
Email: ian.ehrenreich@usc.edu

Abstract

Mutations often have different effects in genetically distinct individuals. Epistasis between mutations and segregating loci is known to be a major contributor to these background effects, but the architecture of these genetic interactions remains largely unknown. Here, we characterize how segregating loci in a cross of two *Saccharomyces cerevisiae* strains impact growth following the deletion of the histone deacetylase *HOS3.* The functions of *HOS3* are not well understood and historically its deletion has shown little effect on reference strains. However, we map two loci that genetically interact with *HOS3* and each other to produce a broad range of responses to the deletion, including near inviability. Although these interactions explain nearly all of the deletion's expressivity, their penetrance depends on a liability threshold involving at least 11 additional nuclear and mitochondrial loci. Multiple lines of evidence imply the deletion uncovers genetically complex changes in translation and genome stability in the mitochondria, suggesting a novel connection between Hos3-mediated deacetylation and the mitochondria. These results provide a valuable example of the complicated and unexpected mechanisms that can cause background effects in genetically diverse populations, and show how characterization of background effects can provide new insights into gene function.

One Sentence Summary

Complex genetics shape a mutation's penetrance and expressivity.

Main Text

Mutations frequently exhibit different effects in genetically distinct individuals (or 'background effects') (*1-3*). Variable expressivity and incomplete penetrance are two of the most prevalent forms of background effects (*4*). Variable expressivity occurs when a mutation shows quantitatively different effects among distinct individuals, while incomplete penetrance occurs when a mutation shows an effect in some individuals but not others (*4*). Variable expressivity and incomplete penetrance are not mutually exclusive; a mutation may only show an effect in certain individuals, but that effect might vary in severity among affected individuals (*4*). Both variable expressivity and incomplete penetrance can arise due to a variety of reasons, including genetic interactions (or epistasis) between a mutation and segregating loci (*4*), environmental influences on a mutation (*4*), and stochastic noise (*5*).

Here, we focus on the contribution of epistasis to expressivity and penetrance. This topic has proven difficult to study, in large part because populations harbor substantial genetic diversity, which can facilitate complex and highly polygenic forms of epistasis with mutations (*6-18*). These genetic interactions are difficult to map in natural populations (*6-18*) and it is unclear how well they are modeled by combinations of lab-induced mutations in otherwise isogenic strain backgrounds (*19, 20*). Fortunately, the budding yeast *Saccharomyces cerevisiae* is a potentially powerful system for studying the expressivity and penetrance of mutations. In this organism, phenotyping of isogenic cell populations under tightly controlled conditions can limit both environmental and stochastic influences on mutations. Moreover, mutations can be easily introduced into genetically diverse yeast strains and crosses, enabling the identification and genetic dissection of background effects (*6, 11, 16-18, 21*).

In this paper, we comprehensively characterize how genetic variants individually and jointly shape the expressivity and penetrance of deletion of the histone deacetylase *HOS3* (*22*) in a yeast cross. We became interested in this gene when, in a screen of 47 complete gene deletions of chromatin regulators, *HOS3* showed epistasis with hundreds of segregating loci in a cross of the reference strain BY4716 ('BY') and the lab strain 322134S ('3S'), which was many more than any other gene examined in that study (Fig. 1A) (*16*). This finding was surprising because, to date, functional genomic screens in BY have found little impact of *HOS3* deletion on growth or other traits (supplementary text 2) (*23*). However, the detection of extensive epistasis between *HOS3* and segregating loci implies that *HOS3* has greater functional significance in BYx3S segregants than

BY. For this reason, we sought to determine how segregating loci genetically interact with the *HOS3* deletion to alter its phenotypic effect.

The HOS3 deletion shows variable expressivity and incomplete penetrance on ethanol

As a starting point, we identified the condition in which the *HOS3* deletion exhibited the greatest variability in phenotypic effects across segregants. Reanalysis of growth data from multiple environments (*16*) found that *HOS3* deletion resulted in the largest increase in phenotypic variance among BYx3S F_2 segregants grown on agar plates containing ethanol as the carbon source (hereafter, 'ethanol'; Fig. 1, A and B and table S1). In this condition, phenotypic variance was more than seven-times higher among *hos3*Δ segregants than wild type segregants, with *hos3*Δ segregants showing a spectrum of growth levels ranging from wild type to near inviability (Fig. 1B and fig. S1). Whereas none of the wild type segregants exhibited very poor growth, 19% (43 out of 221) of the *hos3*Δ segregants were nearly inviable, suggesting that *HOS3* deletion uncovered both quantitative and qualitative phenotypic variation among segregants. These findings indicate that examination of *HOS3* deletion on ethanol provides an opportunity to study how segregating loci modify expressivity and penetrance.

*Expressivity of hos3*Δ *is mostly explained by a cryptic allele in the mitochondrial ribosome*

A linkage scan was performed to identify individual loci influencing the expressivity of the *HOS3* deletion in ethanol. This scan was conducted using 164 wild type and 221 *hos3*Δ F_2 segregants from Mullis et al. (*16*), and detected a single locus on Chromosome IV ($p = 2.54 \times 10^{-54}$; Fig. 1C), at which *hos3*Δ segregants with the BY allele exhibited worse growth than segregants with the 3S allele (Fig. 1D). This locus explained the majority of the phenotypic variance among *hos3*Δ segregants (ANOVA, $R^2 = 0.74$), but accounted for no phenotypic variance among wild type segregants (ANOVA, $R^2 = 0$). Thus, the major determinant of the expressivity of the *HOS3* deletion is a cryptic allele (*24, 25*) that is uncovered in a *hos3*Δ background (supplementary text 3).

Analysis of recombination breakpoints among *hos3*Δ segregants resolved the Chromosome IV locus to five nucleotides—four SNPs in the bidirectional promoter between *MRP20* and *RPB7*, and one nonsynonymous SNP in *MRP20* (Fig. 1E). Differential gene expression analysis and allele-specific expression analysis in wild type and *hos3*Δ BY/3S diploids found no evidence for *HOS3*-mediated transcriptional changes at either of these genes (tables S2 to S3). This suggests that the nonsynonymous SNP in *MRP20*, which respectively encodes a glutamine in BY and an

alanine in 3S at amino acid 105, is causal. We confirmed the causality of *MRP20* using reciprocal hemizygosity analysis (*26*), which showed that the $MRP20^{BY}$ allele resulted in a substantial decrease in growth in the presence of *hos3*Δ (Fig. 1F). Mrp20 is an essential, nuclear-encoded subunit of the mitochondrial ribosome, suggesting we have identified a novel connection between Hos3-mediated deacetylation and mitochondrial translation.

*A three-way genetic interaction accounts for the remainder of hos3*Δ *expressivity*

Next, we performed additional genome-wide linkage scans to identify loci that individually explained the remaining portion of the phenotypic variance among *hos3*Δ segregants. However, this failed to identify any loci with substantial effects (supplementary text 4). To further explain the phenotypic variance among *hos3*Δ segregants, we scanned for loci that show three-way epistasis with *HOS3* and *MRP20*. This identified a single locus on Chromosome XIV ($p = 9.62 \times 10^{-11}$; Fig. 2A and supplementary text 5), at which the BY allele reduced growth in both wild type and *hos3*Δ segregants, but to a greater degree among *hos3*Δ segregants (Fig. 2B). The additive and epistatic effects of *MRP20* and the Chromosome XIV locus collectively explained 88% of the phenotypic variance among *hos3*Δ segregants (ANOVA, R^2) and accounted for all observed cases of *hos3*Δ-mediated near inviability (Fig. 2C). Thus, nearly all of the expressivity of the *HOS3* deletion is explained by its two- and three-way genetic interactions with *MRP20* and Chromosome XIV.

Mechanistic insight into epistasis between *HOS3*, *MRP20*, and the Chromosome XIV locus was limited by poor mapping resolution (supplementary text 5). To more finely resolve the Chromosome XIV locus, we crossed a *hos3*Δ $MRP20^{BY}$ XIV^{BY} F_2 segregant to a *hos3*Δ $MRP20^{BY}$ XIV^{3S} F_2 segregant. 361 F_3 progeny were genotyped by low coverage whole genome sequencing and phenotyped for growth on ethanol, and linkage mapping for additive loci was performed (Fig. 2D). An additive scan was performed because, with *hos3*Δ and $MRP20^{BY}$ fixed in this cross, we expected the Chromosome XIV locus to act in an additive manner. This analysis identified the Chromosome XIV locus at a p-value of 2.50×10^{-43} and resolved this locus to a window spanning all or part of six genes (Fig. 2E, figs. S2 to S4, table S4, and supplemental text S6). Analysis of recombination breakpoints at the Chromosome XIV locus delimited it to a single SNP, which resides in the coding region of *MKT1* (Fig. 2F). This SNP results in a glycine in BY and a serine in 3S at amino acid 30. This exact variant was previously shown to play a role in mitochondrial genome stability in BY (*27*). When considered with *MRP20*, identification of the $MKT1^{BY}$ allele implies that *hos3*Δ lethality results from mitochondrial dysfunction, which should impair growth on non-fermentative carbon sources, such as ethanol.

Epistasis between HOS3, *MKT1*, and *MRP20 impacts mitochondrial genome stability*

While *MKT1* and *MRP20* together largely explain the expressivity of the *HOS3* deletion on ethanol, the fact that the BY allele is inferior at each gene suggests the BY *hos3*Δ strain should grow poorly on ethanol. However, as mentioned previously, a large body of genome-wide screens conducted in the BY reference strain contradict this assertion, as they indicate that *HOS3* deletion has little impact on growth in most conditions, including on ethanol (*23*). To confirm this assertion, we generated and phenotyped BY and 3S *hos3*Δ strains ourselves. This found that the *HOS3* deletion had no measurable effect on growth on ethanol in either cross parent (Fig. 3A).

Identification of *MKT1* and *MRP20*, as well as the fact that our assays were conducted in a respiratory growth environment, implicates impaired mitochondrial function as the cause of near inviability among *hos3*Δ segregants with particular genetic backgrounds. In yeast, functional impairment of mitochondrial translation often results in mitochondrial genome instability, leading to the formation of *petite* colonies that show poor cellular respiration (*28, 29*). *Petite* formation is known to quantitatively vary across strains and is elevated in BY (*27*). For this reason, we measured the frequency of *petite* formation in the wild type and *hos3*Δ BY and 3S strains. In this experiment, the BY *hos3*Δ strain exhibited a roughly three-fold increase in mitochondrial genome instability relative to the BY wild type strain, demonstrating that *HOS3* deletion does in fact have an effect in BY, even though this effect on mitochondrial genome instability does not exhibit a measurable impact on colony growth (Fig. 3B). No such effect of *HOS3* on mitochondrial genome stability was seen in 3S.

We also examined mitochondrial genome instability among wild type and *hos3*Δ F_2 segregants carrying different combinations of alleles at *MKT1* and *MRP20*. This revealed that $MKT1^{BY}$ and $MRP20^{BY}$ jointly produced a substantial increase in mitochondrial genome instability when *HOS3* was deleted, but not while *HOS3* was present (Fig. 3C). Most of these *hos3*Δ segregants showed levels of genome instability around 100%. Thus, although *HOS3* deletion has a significant effect on mitochondrial genome stability in BY, it often has a three-times greater effect on $MKT1^{BY}$ $MRP20^{BY}$ F_2 segregants (Figs. 3B and C). This suggests that BY carries additional alleles that suppress epistasis between *HOS3*, *MKT1*, and *MRP20*. Crossing BY and 3S must have produced segregants that carry 3S alleles at some of the involved loci, disrupting suppression of *HOS3-MKT1-MRP20* genetic interactions.

Penetrance of hos3Δ is governed by a polygenic liability threshold

To identify loci affecting the penetrance of the *HOS3-MKT1-MRP20* genetic interactions, we backcrossed two genetically distinct *hos3Δ* $MKT1^{BY}$ $MRP20^{BY}$ F_2 segregants to BY (Fig. 3A). The resulting 127 F_2B segregants were genotyped by low coverage whole genome sequencing and phenotyped for growth on ethanol. Across the two backcrosses, ~27% (16 of 59) of the *hos3Δ* F_2B segregants showed near inviability, while ~73% (43 of 59) of the *hos3Δ* F_2B segregants exhibited qualitatively better growth (Fig. 3E). Because the ratio of the two phenotypic classes was roughly 3:1, these numbers suggest that, at minimum, two loci are involved in suppression of near inviability in the BY *hos3Δ* strain. However, genetic analysis of the F_2B segregants failed to identify any individual locus or pair of loci that explained the observed phenotypes, suggesting that suppression in fact involves more than two loci (supplementary text 7).

As a next step, we merged all data from F_2, F_3, and F_2B $MRP20^{BY}$ $MKT1^{BY}$ segregants, including some segregants that carried a functional *HOS3* but possessed other gene deletions from Mullis et al. (*16*). This resulted in a meta-dataset of 422 segregants: 270 and 152 of which were *HOS3* and *hos3Δ*, respectively. Each segregant was classified as viable or nearly inviable, using thresholds specific to each type of segregant. Logistic regression was then used to identify loci influencing the penetrance of the *HOS3-MKT1-MRP20* genetic interactions. This identified 11 loci at a conservative permutation-based threshold (Fig. 4A and table S5). At each locus, higher penetrance was observed in the presence of the 3S allele. The genetic interactions between *HOS3*, *MKT1*, and *MRP20* were fully penetrant when at least seven 3S alleles were present across the 11 loci and showed incomplete penetrance among segregants carrying fewer 3S alleles (Fig. 4B and C, and fig. S5). A sigmoidal, rather than a linear, relationship best explained the observed relationship between increasing 3S alleles and penetrance (fig. S6). This implies that the 11 loci establish a liability threshold that determines the penetrance of the *HOS3-MKT1-MRP20* genetic interactions (Fig. 4C and figs. S5 to S6). Due to limitations of the meta-dataset and the fact that treating the 11 loci as having equal, additive effects on the sigmoid provided a strong fit to the data, we did not examine whether the 11 loci interact with each other. However, such analysis would be worthwhile in the future with a larger dataset.

Nuclear and cytoplasmic loci contribute to the liability threshold

10 of the loci involved in the liability threshold were located in the nuclear genome, while one was resided in the mitochondrial genome (Fig. 4, A and D and table S5). Recombination breakpoints delimited eight of the 10 nuclear loci to between one and three candidate genes (fig. S7 and table

S5). Among the five loci detected at single gene resolution, three were nuclear-encoded mitochondrial proteins: the cytochrome C heme lyase *CYC3*, the mitochondrial ribosome component *MRP8*, and the mitochondrial outer membrane component *YSC83*. The other two were the RNA helicase *ECM16* and the alpha-tubulin *TUB3*. The most common functional grouping among the remaining loci was chromatin regulation, as reflected by the identification of HDA1 histone deacetyltransferase subunit (*HDA2*), a copy of histone H3 (*HHT1*), and a copy of histone H4 (*HHF1*), though another subunit of the mitochondrial ribosome was also present (*MHR1*).

The identified loci also suggest that cytonuclear genetic interactions influence the penetrance of the *HOS3-MKT1-MRP20* genetic interactions, as one of the detected loci was located in the mitochondrial genome. Notably, past work implicated a contribution of mitochondrial genotype to some background effects in yeast, but did not identify involved loci (*30*). Here, high resolution mapping of the mitochondrial locus was possible because 59 distinct recombinant mitochondrial haplotypes were present in the meta-dataset. Recombination breakpoints delimited the mitochondrial locus to the promoter and coding region of the 15S rRNA, which encodes a structural RNA component of the small subunit of the mitochondrial ribosome ($p = 3.96 \times 10^{-7}$; Fig. 4, D and F). Additionally, we observed a second mitochondrial peak that narrowly fell below the permutation-based significance threshold ($p = 1.73 \times 10^{-4}$ vs. threshold = 1.30×10^{-4}; Fig. 4D and supplementary text 8). This second mitochondrial locus did not exhibit linkage disequilibrium with the 15S rRNA, suggesting it represented a distinct mitochondrial influence on the penetrance of the *HOS3-MKT1-MRP20* genetic interactions (Fig. 4E). This locus was delimited to two nucleotides in the promoter of the mitochondrial asparagine tRNA (Fig. 5F and supplementary text 8), providing further support that *HOS3* deletion impacts mitochondrial translation.

Discussion

This paper describes one of the first near complete genetic characterizations of any mutation's expressivity and penetrance. Focusing on *HOS3*, a gene whose deletion whose deletion was historically though to have little phenotypic effect (*23*), we showed a substantial increase in phenotypic variance among *hos3*Δ segregants. Response to the mutation is influenced by at least 13 loci in total: two govern most of the mutation's expressivity, while the additional 11 or more influence the penetrance of genetic interactions between *HOS3*, *MKT1*, and *MRP20*. When all of these 13 loci are fixed for alleles from the same parent, the mutation has no effect on growth and little to no effect on mitochondrial genome stability. This allele configuration is non-random

(binomial test, p = 0.0002), raising the prospect that the expressivity and penetrance of the *HOS3* deletion may be shaped by co-evolved alleles in one or both of the parents that were shuffled during meiosis. Given that the majority of the detected loci harbor genes involved in mitochondrial translation and mitochondrial genome stability, any such co-evolution may have involved selection on mitochondrial function.

Our work also shows how studying background effects can provide new insights into gene function. *HOS3* is a fungal-specific gene (*31*) that was originally annotated as a histone deacetylase based on its similarity to the canonical histone deacetylase Hda1 (*32*). However, *in vivo* experiments have failed to detect physical interactions between Hos3 and histones and have found that *HOS3* deletion alters acetylation at only one genomic region—the rDNA locus (*33*). This raises questions about the role of Hos3 in the nucleus, suggesting that the enzyme may in fact function elsewhere in the cell. Consistent with this possibility, Hos3 is mainly present in the cytoplasm and bud neck (*34*), indicating it may in fact act as a cytoplasmic lysine deacetylase. Supporting such a cellular role, Hos3 was recently found to deacetylate nuclear pore proteins at the perinuclear membrane of daughter cells, thereby impacting nuclear transport and cell cycle progression (*35*). Our findings suggest that Hos3 has another role outside the nucleus, as it impacts the function of multiple components of the mitochondrial translation machinery. Although the experiments described here do not clarify whether Hos3 acts in the mitochondrial compartment itself, recent evidence suggests that Hos3 is present in the mitochondria at a low concentration (*36*).

Additionally, in conclusion, the genetic complexity we have found here may inform efforts to understand expressivity and penetrance in other model systems, including humans. For example, there is great interest in determining why certain people do not show the phenotypic effects of highly penetrant alleles that are known to cause disease (*3, 37, 38*). Our study shows that such resilience may involve a large number of loci, which may be distributed throughout both the nuclear and organellar genomes. Our work also suggests that the loci that govern expressivity and penetrance may not be predictable based on current knowledge of mutated genes and their functions. This speaks to the complicated and unexpected forms of epistasis that can arise between mutations and segregating loci due to the tremendous genetic diversity harbored within populations (*6-18*). It also illustrates the importance of continuing to characterize the forms of epistasis (*39-47*), including background effects, that occur in natural populations, as these forms of genetic interactions are immediately relevant to evolution and disease, and may not emerge

from other types of studies that do not directly interrogate natural variation in genetically diverse populations.

Funding

This work was funded by grants R01GM110255 and R35GM130381 from the National Institutes of Health to I.M.E., as well as Research Enhancement Fellowships from the University of Southern California Graduate School to R.S. and M.N.M.

Author Contributions

R.S. and I.M.E. conceptualized this project. R.S., M.N.M., T.M., and R.F. performed the experiments. R.S. and I.M.E. analyzed the data. R.S. and I.M.E. wrote the paper. R.S., M.N.M., T.M., R.F., and I.M.E. edited the manuscript.

Competing Interests

The authors declare no competing interests.

Data and materials availability

All data used in this manuscript is included in the Supplementary Materials.

Acknowledgements

We thank Gareth Cromie and Aimée Dudley for input at an early stage of this project, Jenna Sloan and Aarohi Mahableshwarkar for assistance with experiments, and Alessandro Coradini, Ilan Goldstein, Joseph Hale, and Cara Hull for feedback during the implementation and writing phases of this work.

References

1. J. H. Nadeau, Modifier genes in mice and humans. *Nat Rev Genet* **2**, 165-174 (2001).

2. C. H. Chandler, S. Chari, I. Dworkin, Does your gene need a background check? How genetic background impacts the analysis of mutations, genes, and evolution. *Trends Genet* **29**, 358-366 (2013).

3. J. D. Riordan, J. H. Nadeau, From peas to disease: modifier genes, network resilience, and the genetics of health. *Am J Hum Genet* **101**, 177-191 (2017).

4. A. J. F. Griffiths, S. R. Wessler, S. B. Carroll, J. Doebley, *Introduction to genetic analysis*. (Macmillian Publishers, New York, NY, ed. 12th, 2015).

5. A. Raj, S. A. Rifkin, E. Andersen, A. van Oudenaarden, Variability in gene expression underlies incomplete penetrance. *Nature* **463**, 913-918 (2010).

6. R. D. Dowell *et al.*, Genotype to phenotype: a complex problem. *Science* **328**, 469 (2010).

7. S. Chari, I. Dworkin, The conditional nature of genetic interactions: the consequences of wild-type backgrounds on mutational interactions in a genome-wide modifier screen. *PLoS Genet* **9**, e1003661 (2013).

8. C. H. Chandler, S. Chari, D. Tack, I. Dworkin, Causes and consequences of genetic background effects illuminated by integrative genomic analysis. *Genetics* **196**, 1321-1336 (2014).

9. A. B. Paaby *et al.*, Wild worm embryogenesis harbors ubiquitous polygenic modifier variation. *Elife* **4**, (2015).

10. M. B. Taylor, I. M. Ehrenreich, Genetic interactions involving five or more genes contribute to a complex trait in yeast. *PLoS Genet* **10**, e1004324 (2014).

11. M. B. Taylor, I. M. Ehrenreich, Transcriptional derepression uncovers cryptic higher-order genetic interactions. *PLoS Genet* **11**, e1005606 (2015).

12. V. Vu *et al.*, Natural variation in gene expression modulates the severity of mutant phenotypes. *Cell* **162**, 391-402 (2015).

13. M. B. Taylor, J. Phan, J. T. Lee, M. McCadden, I. M. Ehrenreich, Diverse genetic architectures lead to the same cryptic phenotype in a yeast cross. *Nat Commun* **7**, 11669 (2016).

14. J. T. Lee, M. B. Taylor, A. Shen, I. M. Ehrenreich, Multi-locus genotypes underlying temperature sensitivity in a mutationally induced trait. *PLoS Genet* **12**, e1005929 (2016).

15. C. H. Chandler *et al.*, How well do you know your mutation? Complex effects of genetic background on expressivity, complementation, and ordering of allelic effects. *PLoS Genet* **13**, e1007075 (2017).

16. M. N. Mullis, T. Matsui, R. Schell, R. Foree, I. M. Ehrenreich, The complex underpinnings of genetic background effects. *Nat Commun* **9**, 3548 (2018).

17. J. Hou, G. Tan, G. R. Fink, B. J. Andrews, C. Boone, Complex modifier landscape underlying genetic background effects. *Proc Natl Acad Sci U S A* **116**, 5045-5054 (2019).

18. J. T. Lee, A. L. V. Coradini, A. Shen, I. M. Ehrenreich, Layers of cryptic genetic variation underlie a yeast complex trait. *Genetics* **211**, 1469-1482 (2019).

19. M. Costanzo *et al.*, A global genetic interaction network maps a wiring diagram of cellular function. *Science* **353**, (2016).

20. E. Kuzmin *et al.*, Systematic analysis of complex genetic interactions. *Science* **360**, (2018).

21. M. Galardini *et al.*, The impact of the genetic background on gene deletion phenotypes in Saccharomyces cerevisiae. *Mol Syst Biol* **15**, e8831 (2019).

22. A. A. Carmen *et al.*, Yeast HOS3 forms a novel trichostatin A-insensitive homodimer with intrinsic histone deacetylase activity. *Proc Natl Acad Sci U S A* **96**, 12356-12361 (1999).

23. J. M. Cherry *et al.*, Saccharomyces Genome Database: the genomics resource of budding yeast. *Nucleic Acids Res* **40**, D700-705 (2012).

24. G. Gibson, I. Dworkin, Uncovering cryptic genetic variation. *Nat Rev Genet* **5**, 681-690 (2004).

25. A. B. Paaby, M. V. Rockman, Cryptic genetic variation: evolution's hidden substrate. *Nat Rev Genet* **15**, 247-258 (2014).

26. L. M. Steinmetz *et al.*, Dissecting the architecture of a quantitative trait locus in yeast. *Nature* **416**, 326-330 (2002).

27. L. N. Dimitrov, R. B. Brem, L. Kruglyak, D. E. Gottschling, Polymorphisms in multiple genes contribute to the spontaneous mitochondrial genome instability of Saccharomyces cerevisiae S288C strains. *Genetics* **183**, 365-383 (2009).

28. A. M. Myers, L. K. Pape, A. Tzagoloff, Mitochondrial protein synthesis is required for maintenance of intact mitochondrial genomes in Saccharomyces cerevisiae. *EMBO J* **4**, 2087-2092 (1985).

29. G. S. Shadel, Yeast as a model for human mtDNA replication. *Am J Hum Genet* **65**, 1230-1237 (1999).

30. M. D. Edwards, A. Symbor-Nagrabska, L. Dollard, D. K. Gifford, G. R. Fink, Interactions between chromosomal and nonchromosomal elements reveal missing heritability. *Proc Natl Acad Sci U S A* **111**, 7719-7722 (2014).

31. P. Trojer *et al.*, Histone deacetylases in fungi: novel members, new facts. *Nucleic Acids Res* **31**, 3971-3981 (2003).

32. S. E. Rundlett *et al.*, HDA1 and RPD3 are members of distinct yeast histone deacetylase complexes that regulate silencing and transcription. *Proc Natl Acad Sci U S A* **93**, 14503-14508 (1996).

33. D. Robyr *et al.*, Microarray deacetylation maps determine genome-wide functions for yeast histone deacetylases. *Cell* **109**, 437-446 (2002).

34. M. Wang, R. N. Collins, A lysine deacetylase Hos3 is targeted to the bud neck and involved in the spindle position checkpoint. *Mol Biol Cell* **25**, 2720-2734 (2014).

35. A. Kumar *et al.*, Daughter-cell-specific modulation of nuclear pore complexes controls cell cycle entry during asymmetric division. *Nat Cell Biol* **20**, 432-442 (2018).

36. A. G. Rocha *et al.*, Nfs1 cysteine desulfurase protein complexes and phosphorylation sites as assessed by mass spectrometry. *Data Brief* **15**, 775-799 (2017).

37. R. Chen *et al.*, Analysis of 589,306 genomes identifies individuals resilient to severe Mendelian childhood diseases. *Nat Biotechnol* **34**, 531-538 (2016).

38. V. M. Narasimhan *et al.*, Health and population effects of rare gene knockouts in adult humans with related parents. *Science* **352**, 474-477 (2016).

39. O. Carlborg, C. S. Haley, Epistasis: too often neglected in complex trait studies? *Nat Rev Genet* **5**, 618-625 (2004).

40. H. Shao *et al.*, Genetic architecture of complex traits: large phenotypic effects and pervasive epistasis. *Proc Natl Acad Sci U S A* **105**, 19910-19914 (2008).

41. T. F. Mackay, Epistasis and quantitative traits: using model organisms to study gene-gene interactions. *Nat Rev Genet* **15**, 22-33 (2014).

42. T. F. Mackay, J. H. Moore, Why epistasis is important for tackling complex human disease genetics. *Genome Med* **6**, 124 (2014).

43. M. L. Siegal, J. Y. Leu, On the nature and evolutionary impact of phenotypic robustness mechanisms. *Annu Rev Ecol Evol Syst* **45**, 496-517 (2014).

44. M. B. Taylor, I. M. Ehrenreich, Higher-order genetic interactions and their contribution to complex traits. *Trends Genet* **31**, 34-40 (2015).

45. S. K. Forsberg, J. S. Bloom, M. J. Sadhu, L. Kruglyak, O. Carlborg, Accounting for genetic interactions improves modeling of individual quantitative trait phenotypes in yeast. *Nat Genet* **49**, 497-503 (2017).

46. I. M. Ehrenreich, Epistasis: searching for interacting genetic variants using crosses. *Genetics* **206**, 531-535 (2017).

47. R. F. Campbell, P. T. McGrath, A. B. Paaby, Analysis of epistasis in natural traits using model organisms. *Trends Genet* **34**, 883-898 (2018).

Figure Legends

Fig. 1. *HOS3* deletion increases phenotypic variability in the BYx3S cross, in large part due to a cryptic genetic variant in the nuclear-encoded, essential mitochondrial ribosomal subunit *MRP20*. (**A**) Wild type and hemizygous BY/3S diploids were generated and sporulated to produce *HOS3* and *hos3*Δ F_2 BYx3S segregants. (**B**) *HOS3* deletion resulted in a large increase in phenotypic diversity among segregants. (**C**) Linkage mapping using the *HOS3* and *hos3*Δ segregants identified a single locus on Chromosome IV that shows a genetic interaction with the *HOS3* deletion. The peak marker was from 1,277,231 to 1,277,959 and the confidence interval extended from position 1,272,164 to position 1,278,407, encompassing (from left to right) part of *URH1* and all of *DIT2*, *DIT1*, *RPB7*, and *MRP20*. (**D**) The BY allele of the Chromosome IV locus has a large effect in *hos3*Δ segregants, but no effect in *HOS3* segregants. (**E**) Recombination breakpoints in *hos3*Δ segregants delimit the Chromosome IV locus to five SNPs (small vertical black lines along the x-axis) in the *RPB7-MRP20* region of the chromosome. Dashed vertical lines show the window delimited by the recombination breakpoints. (**F**) Reciprocal hemizygosity analysis in a *hos3*Δ BY/3S diploid was conducted at closely linked, non-essential genes and found that *MRP20* is the causal gene underlying the Chromosome IV locus. Throughout the paper, blue and orange are used to denote BY and 3S genetic material, respectively. Regarding hemizygotes, black triangles denote the absence of one allele and colored triangles indicate the alleles that are

present. All growth data presented in the paper are measurements of colonies on agar plates containing rich medium with ethanol as the carbon source.

Fig. 2. Epistasis between *HOS3*, *MRP20*, and *MKT1* explains the expressivity of the *HOS3* deletion. (**A**) Linkage mapping in the *HOS3* and *hos3*Δ BYx3S F_2 segregants identifies a locus on Chromosome XIV that shows a three-way genetic interaction with *HOS3* and *MRP20*. (**B**) The Chromosome XIV locus has effects in both *HOS3* and *hos3*Δ segregants but exhibits a bimodal distribution among *hos3*Δ segregants. (**C**) When both *MRP20* and the Chromosome *XIV* locus are considered, the full range of expressivity among segregants is nearly explained. Segregants with BY alleles at both loci are nearly inviable. (**D**) To identify the causal gene at the *XIV* locus, we crossed two *hos3*Δ $MRP20^{BY}$ F_2 segregants that differed at the Chromosome XIV locus and gathered a panel of F_3 segregants. (**E**) Linkage mapping in the F_3 segregants identified the Chromosome XIV locus at high resolution, with a peak at position 467,219. The confidence interval extended from 463,775 to 509,173 and partially or completely included 27 protein-coding genes. Tick marks denote every 100,000 bases along the chromosome. (**F**) Recombination breakpoints in the F_3 segregants delimit the Chromosome XIV locus to a single SNP in *MKT1*. Vertical dashed line highlights the delimited causal polymorphism, while small vertical lines along the x-axis indicate different SNPs in the window that is shown.

Fig. 3. The *HOS3* deletion leads to elevated mitochondrial genome instability in BYx3S segregants, which is partially suppressed by backcrossing. (**A**) Wild type and *hos3*Δ parental strains show comparable growth (95% bootstrap confidence). (**B**) For a given strain, the fraction of cells with mitochondrial genome instability was measured using the frequencies of *petites*. Cells with absent or defective mitochondrial genomes will be unable to generate energy through cellular respiration and thus will produce *petite* colonies. BY has higher rate of *petite* formation than 3S. Also, BY *hos3*Δ strains show an elevated *petite* frequency relative to wild type BY. (**C**) $MKT1^{BY}$ $MRP20^{BY}$ segregants with the *HOS3* deletion show dramatically elevated *petite* frequencies, while all other *HOS3* and *hos3*Δ F_2 segregants exhibit comparable *petite* frequencies to wild type BY and 3S. (**D**) Two genetically distinct *hos3*Δ $MKT1^{BY}$ $MRP20^{BY}$ F_2 segregants were backcrossed to BY to produce F_2B panels. (**E**) Backcrossing produces *hos3*Δ $MKT1^{BY}$ $MRP20^{BY}$ F_2B segregants that mostly exhibit wild type growth, suggesting that increasing the proportion of the genome contributed by BY masks genetic interactions between *HOS3*, *MRP20*, and *MKT1*. Note, backcross 1 showed generally enhanced mitochondrial genome instability relative to wild type BY and backcross 2.

Fig. 4. A liability threshold involving a large number of nuclear and mitochondrial loci determines the penetrance of the *HOS3-MKT1-MRP20* genetic interactions. (**A**) We combined all *MKT1*^{BY} *MRP20*^{BY} segregants from the F_2, F_3, and F_2B panels, binarized each segregant as viable or nearly inviable based on panel-specific thresholds, and then identified 11 loci that interact with *HOS3* using a logistic regression model. (**B**) Growth as a function of the number of 3S alleles each individual carries at these loci is plotted. Which panel each segregant came from is also indicated. Note, the distribution of F_2 segregants are slightly right-shifted relative to expectations due to the non-random segregation of three loci, fixation for the 3S allele at *ECM16,* enrichment for 3S loci at the first mitochondrial locus, and enrichment for the 3S allele at the Chromosome XVI locus that is 53,010 kb downstream from *HOS3* (Fig. S5). The non-randomness at these loci occurred at the stage of spore generation not phenotyping on ethanol, but importantly these loci all segregate in the meta-dataset. (**C**) The number of 3S alleles at the identified loci shows a sigmoidal relationship with the penetrance of the *HOS3-MKT1-MRP20* interactions, indicating these loci form a liability threshold. 95% bootstrap confidence intervals are provided. (**D**) Significance of the interaction term in A is shown exclusively for the mitochondrial genome, illustrating not only the mitochondrial locus detected among the 11 mentioned above but also a second locus just below the permutation threshold. The peak position at the first locus extends from 1,279 to 6,971 and the peak spans two nucleotides from 67,965-67,966. (**E**) Linkage disequilibrium (r^2) indicates the two mitochondrial loci are distinct. For each locus, r^2 between the peak marker and all other SNPs in the mitochondrial genome is shown. (**F**) The genomic context for each mitochondrial locus is shown, suggesting both mitochondrial loci impact mitochondrial translation: the first locus encodes the 15S mRNA of the mitochondrial ribosome and the other corresponds to the mitochondrial asparagine tRNA. Vertical black lines denote the genetic variants that exhibit the same minimal p-value at each locus.

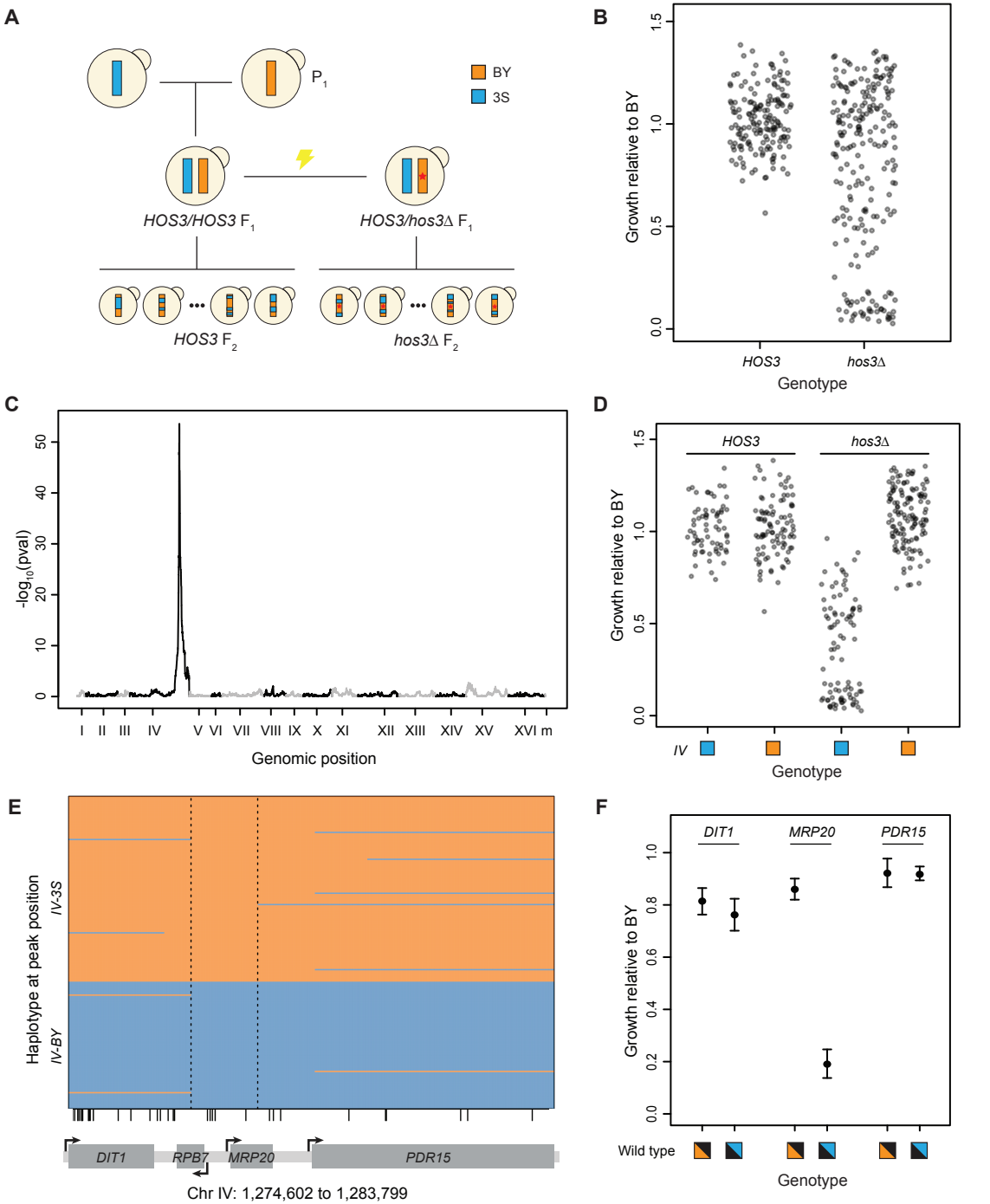
A
P1
BY
3S
HOS3/HOS3 F1
HOS3/hos3Δ F1
HOS3 F2
hos3Δ F2
B
Growth relative to BY
0.0
0.5
1.0
1.5
HOS3
hos3Δ
Genotype
C
-log10(pval)
0
10
20
30
40
50
I II III IV V VI VII VIII IX X XI XII XIII XIV XV XVI m
Genomic position
D
HOS3
hos3Δ
Growth relative to BY
0.0
0.5
1.0
1.5
IV
Genotype
E
Haplotype at peak position
IV-3S
IV-BY
DIT1
RPB7
MRP20
PDR15
Chr IV: 1,274,602 to 1,283,799
F
DIT1
MRP20
PDR15
Growth relative to BY
0.0
0.2
0.4
0.6
0.8
1.0
Wild type
Genotype

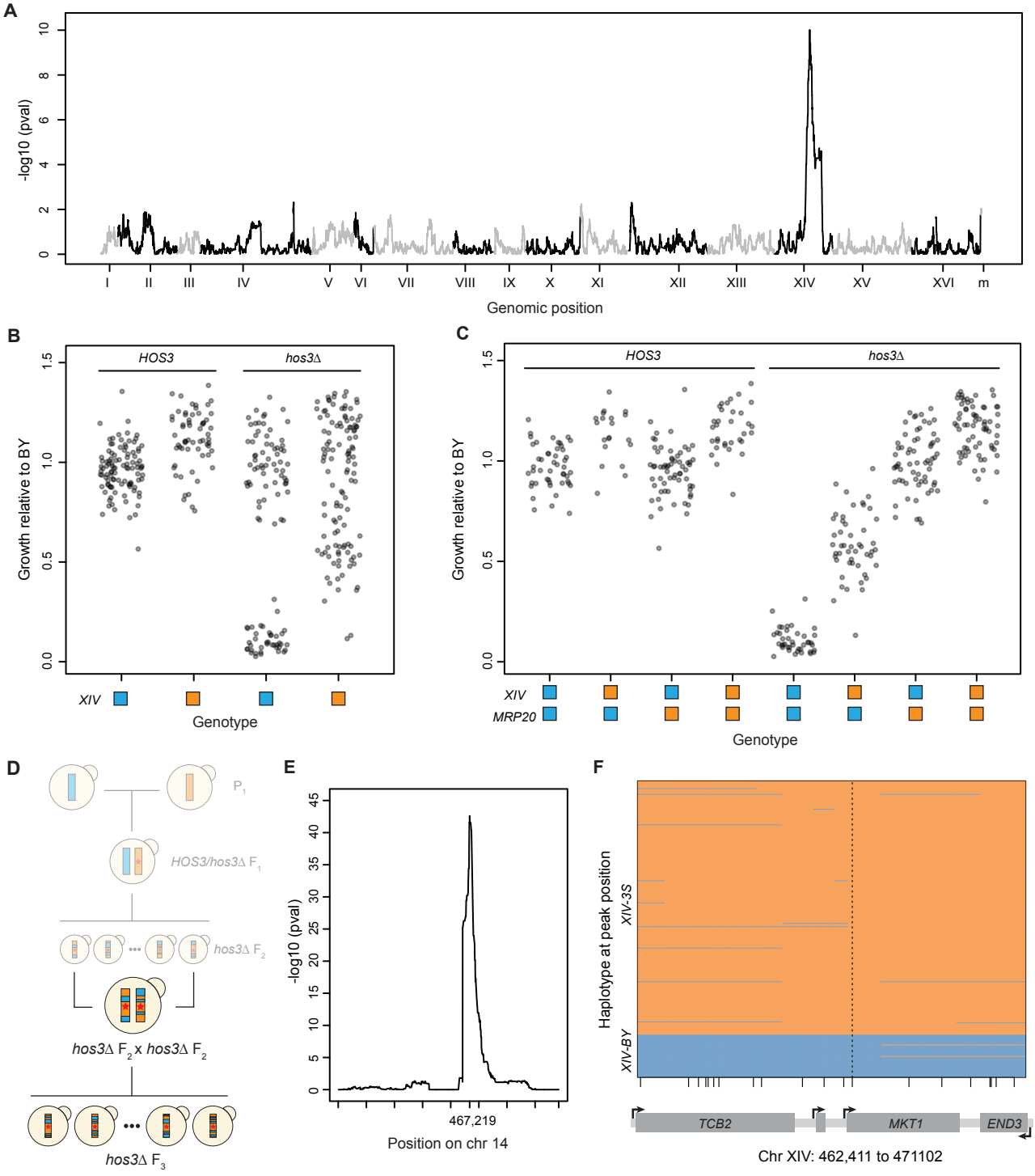
A
-log10 (pval)
0
2
4
6
8
10
I
II
III
IV
V
VI
VII
VIII
IX
X
XI
XII
XIII
XIV
XV
XVI
m
Genomic position
B
HOS3
hos3Δ
Growth relative to BY
0.0
0.5
1.0
1.5
XIV
Genotype
C
HOS3
hos3Δ
Growth relative to BY
0.0
0.5
1.0
1.5
XIV
MRP20
Genotype
D
P1
HOS3/hos3Δ F1
hos3Δ F2
hos3Δ F2 x hos3Δ F2
hos3Δ F3
E
-log10 (pval)
0
5
10
15
20
25
30
35
40
45
467,219
Position on chr 14
F
Haplotype at peak position
XIV-3S
XIV-BY
TCB2
MKT1
END3
Chr XIV: 462,411 to 471102

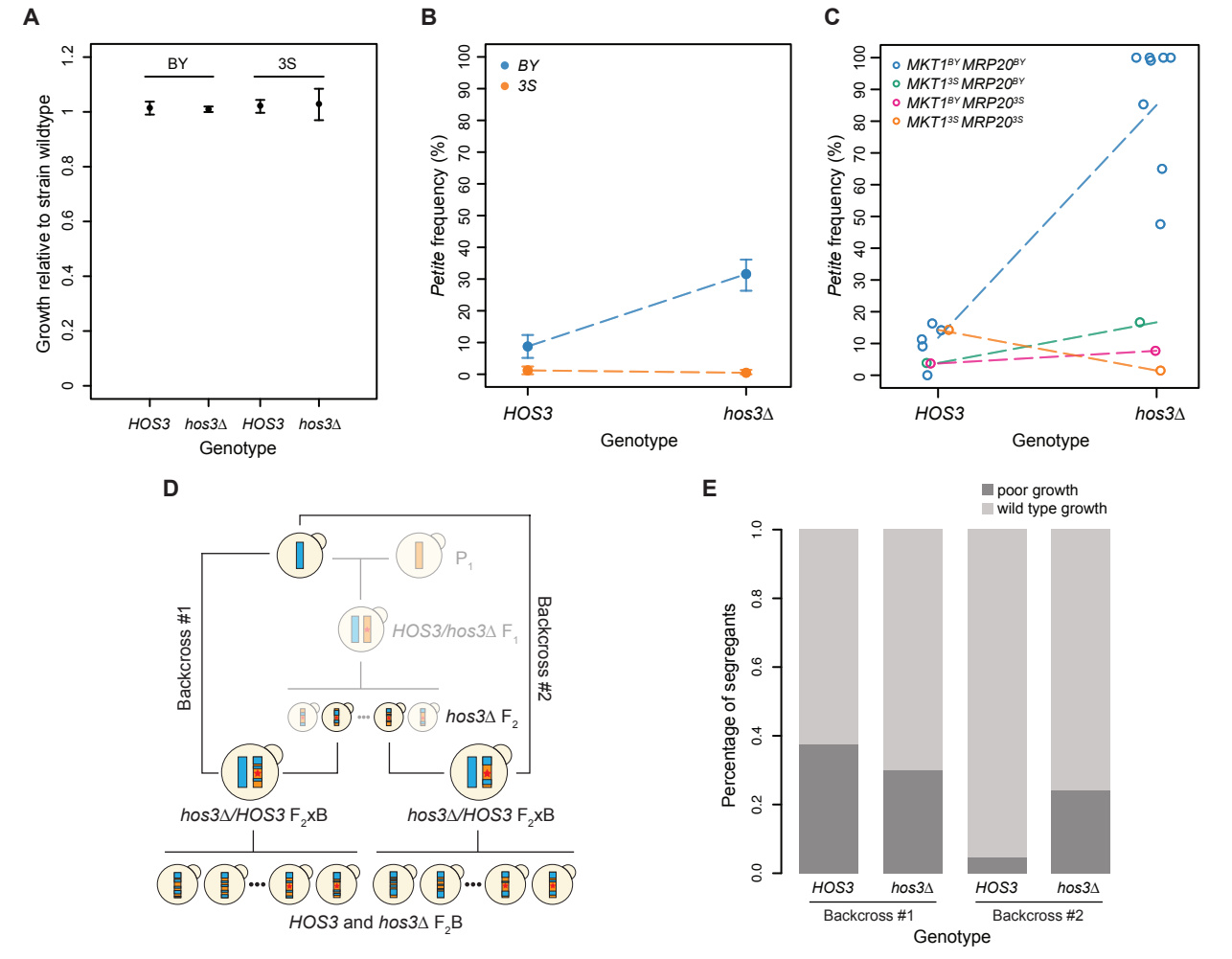
A
BY
3S
Growth relative to strain wildtype
HOS3
hos3Δ
HOS3
hos3Δ
Genotype
B
BY
3S
Petite frequency (%)
HOS3
hos3Δ
Genotype
C
MKT1BY MRP20BY
MKT1 3S MRP20BY
MKT1BY MRP203S
MKT1 3S MRP203S
Petite frequency (%)
HOS3
hos3Δ
Genotype
D
P1
HOS3/hos3Δ F1
hos3Δ F2
Backcross #1
Backcross #2
hos3Δ/HOS3 F2xB
hos3Δ/HOS3 F2xB
HOS3 and hos3Δ F2B
E
poor growth
wild type growth
Percentage of segregants
HOS3
hos3Δ
HOS3
hos3Δ
Backcross #1
Backcross #2
Genotype

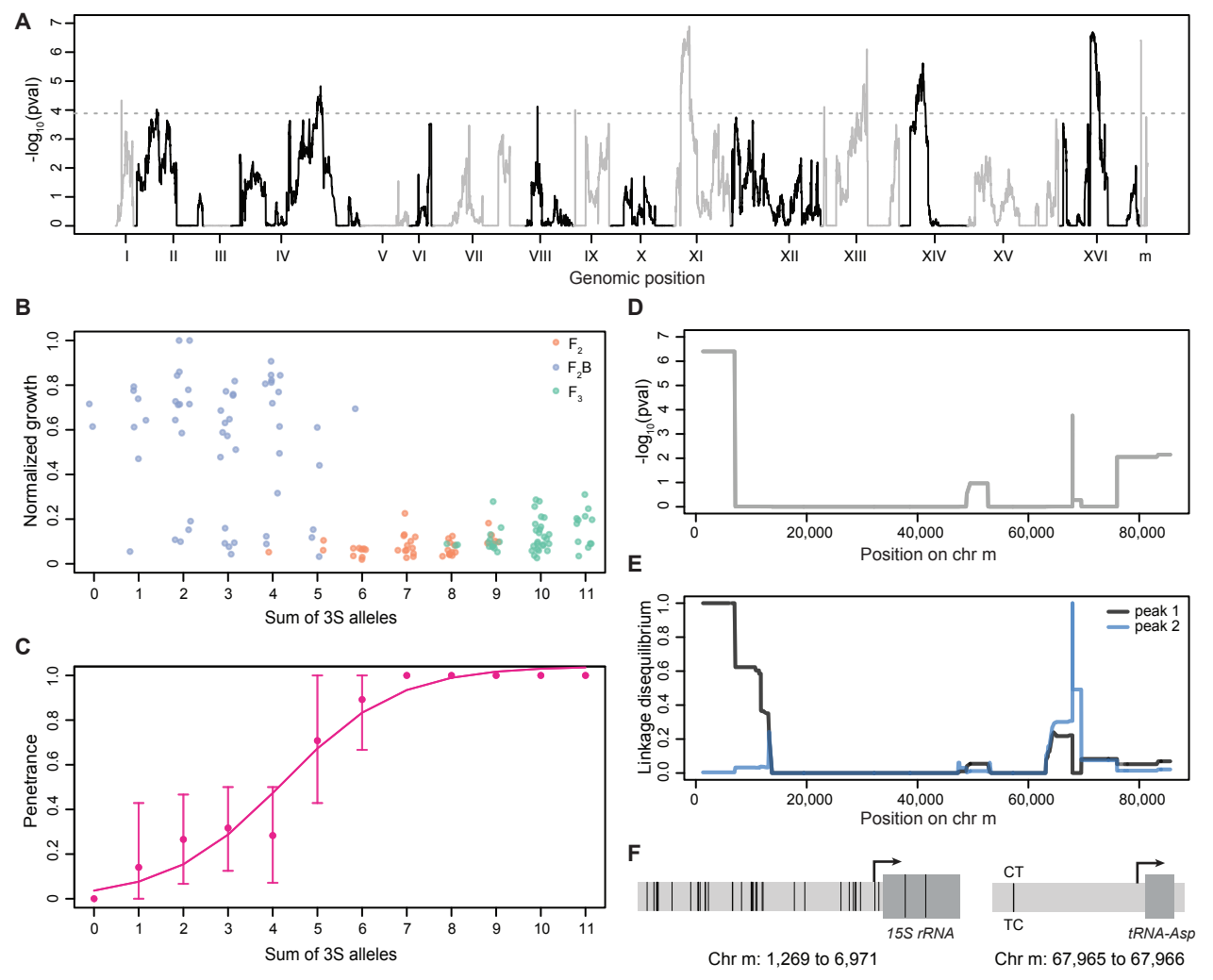
A
-log10(pval)
Genomic position
I
II
III
IV
V
VI
VII
VIII
IX
X
XI
XII
XIII
XIV
XV
XVI
m
B
Normalized growth
Sum of 3S alleles
F2
F2B
F3
C
Penetrance
Sum of 3S alleles
D
-log10(pval)
Position on chr m
E
Linkage disequilibrium
peak 1
peak 2
Position on chr m
F
15S rRNA
CT
TC
tRNA-Asp
Chr m: 1,269 to 6,971
Chr m: 67,965 to 67,966